JOURNAL OF AIRCRAFT
Vol. 43, No. 6, November–December 2006

Post-Stall Flow Control of Sharp-Edged Wings via Unsteady Blowing

Jose M. Rullan,* Pavlos P. Vlachos,† and Demetri P. Telionis‡
Virginia Polytechnic Institute and State University, Blacksburg, Virginia 24061
and
Matthew D. Zeiger§
Aeroprobe Corporation, Blacksburg, Virginia 24060

DOI: 10.2514/1.19495

In previous publications we reported on how leading-edge oscillating miniflaps can control separated flows over sharp-edged airfoils. In this paper we extend our efforts and present results on the control of flows over such airfoils using unsteady minijets deployed along the leading edge. We developed and employed a new design of an unsteady jet actuator that can achieve a wide range of blowing frequencies, allowing the independent control of the jet amplitude. The results indicate that unsteady minijet actuation is as effective as leading-edge miniflaps. The management of separated flow generates in the average lift increases the order of 50%. The present data are compared with results obtained with large, fixed leading-edge flaps. This implies that heavy flaps and the accompanied hydraulics necessary for takeoff, landing, and maneuvering could be replaced with flow control devices.

Nomenclature

Cp	=	pressure coefficient $= P_{\text{local}}/\frac{1}{2}\rho U_\infty^2$
$C\mu$	=	momentum coefficient $= \rho_{\text{jet}} u_{\text{jet}} H/\rho_\infty U_\infty c \sin\alpha$
c	=	chord
F	=	dimensionless actuation frequency $= f_{\text{actuation}}/f_{\text{shedding}}$
$f_{\text{actuation}}$	=	actuation frequency
f_{shedding}	=	natural shedding frequency
H	=	slot width
St	=	Strouhal number Strouhal number $= f_{\text{shedding}} c \sin(\alpha)/U_\infty$
U_{rms}	=	maximum rms velocity
U_∞	=	characteristic freestream velocity
u_{jet}	=	maximum jet exit velocity
x/c	=	chordwise downstream distance
y, z	=	coordinates attached to nozzle, Fig. 4
α	=	angle of attack
ρ	=	density of air

I. Introduction

STEALTH fighters and supersonic transport aircraft require sharp-edge configurations and in particular, sharp-edged wings. These wings, however, are very inefficient in takeoff and landing, requiring high speeds and long runways. The aerodynamic performance of sharp-edged wings is very poor at low speeds, because the flow separates over the leading edges, even at low angles of attack, with detrimental effects such as increase in drag, decrease in lift, and reduction in aircraft maneuverability. Flow control may be an option, and the present authors have demonstrated that indeed, this technique could improve the aerodynamic performance of sharp-edged wings (Miranda et al. [1,2]).

Presented as Paper 62 at the 41st Aerospace Sciences Meeting and Exhibit, Reno, NV, 6–9 January 2003; received 15 August 2005; revision received 14 March 2006; accepted for publication 20 March 2006.

*Graduate Student. Member AIAA.
†Assistant Professor. Member AIAA.
‡Professor, Associate Fellow. Member AIAA.
§CEO, Senior Scientist, Virginia Tech Corporate Research Center. Member AIAA.

Sharp-edged airfoils suffer from separation even at low angles of attack such as 6 deg, because the flow cannot negotiate the sharp turn at the leading edge. With flow separation over both the leading and the trailing edge, the airfoil behaves as a bluff body. The interest in the present study is to control separated flow, not flow separation. With the implementation of flow control techniques, improvements in the lift coefficient can be obtained in a time-averaged sense. This is achieved by controlling vortex shedding by mixing enhancement of high momentum flow from the freestream with low momentum flow in the separated region. In the process, vortices are better organized and form closer to the wing surface. This mechanism is known as vortex-induced lift.

Zhou et al. [3] were the first to try to control the fully separated flow over a sharp-edged airfoil. They used a rounded-edge airfoil placed backwards in a wind tunnel, so that the sharp trailing edge faced the oncoming flow. Their tests were carried out only at 27 deg angle of attack, but their results indicated that an increase in lift could be achieved. Hsiao et al. [4] employed a pulsed microflap on the rounded leading edge of a wing to control fully separated flow. They focused on the position, amplitude, and frequency of the flap motion necessary to improve the aerodynamic characteristics of the flow over airfoils at high angles of attack. Hsiao and Wang found that periodic perturbations can organize and enhance the average strength of the shedding vortices, and can increase the lift in a time-average sense by as much as 50%. Hsiao et al. [5] later made modifications to their previous design, finding that the most effective excitation corresponds to a flap motion activated at the vortex-shedding frequency. They also found that larger amplitudes of excitation motion produced a larger lift coefficient.

Miranda et al. [1,2] tested a wing with sharp leading and trailing edges and circular-arc surfaces. This configuration is very close to the wings employed by most modern fighter aircraft. To create the necessary flow disturbance, Miranda et al. [1,2] used a small oscillating flap placed on the leading edge of their airfoil. They showed an increase in lift in the average of up to 70%. But the flap must penetrate through the separated region in order to have any effect on the formation of vortices. This is believed to be the reason why the effect was greatly reduced as the angle of attack was increased. Miranda and his coworkers also found that the effectiveness of oscillating flaps is not limited in the frequency domain. Indeed, they demonstrated that an oscillating flap could generate a wide range of effective frequencies for the control of separated flow over a sharp-edge airfoil. But oscillating miniflaps may not be attractive to the aircraft designers. In the present paper we

discuss our efforts to use oscillating blowing instead of mechanical flaps to generate a small disturbance and control the flow over sharp-edged wings.

Steady and oscillatory blowing have been studied extensively as methods of flow control but not over sharp leading edges. Seifert et al. [6] examined oscillatory blowing on the trailing-edge flap of a NACA-0015 airfoil. They used a NACA-0015 airfoil with a trailing-edge flap equipped with jets in the form of a 2-D slot on its upper surface above the hinge. They concluded that steady blowing had no effect on lift or drag. However, modulating blowing generated an increase in lift and cut the drag in half McManus and Magill [7] studied separation control using pulsed jets over airfoils with rounded leading edges and found that for a $\alpha \leq 10$ deg pulsed jets caused an increase in lift of up to 50% over a base line case. Seifert and Pack [8] provide strong evidence that such methods are applicable to flows at high Reynolds numbers, the order of 40 million and high subsonic Mach numbers ($M = 0.6$). The flow over their model was always separated and the separation location was not affected by the flow control mechanism.

Synthetic jets [9], and in particular, jets generated by piezoelectric actuators [10–12] have also been employed to control the flow. A typical example is the one by Cattafesta et al. [10], where one sheet of piezoceramic was attached to the underside of a shim. Synthetic jet actuators based on cavity designs and driven by piezoelectric devices are most efficient at the resonance frequency of the piezo and limited by the natural frequency of the cavity [11,12]. The rms of the velocity they generate drops off sharply away from the preferred frequencies. Such actuators have proven very useful in the laboratory but may not be as effective in practice. Recognizing these facts, Gilarranz and Rediniotis [13] designed an actuator consisting essentially of small positive-displacement machines. They tested a NACA0015 wing with rounded leading edges containing six reciprocating compressors, which were driven by two dc motors. These compressors/pistons created a synthetic jet (zero mean mass flux) that was efficient in the entire range of the possible actuation frequencies. They found that flow separation control was effective at angles of attack and freestream velocities as high as 25 deg and 45 m/s, respectively. The drawback of such actuators is the complexity of the device. In the present paper we describe a very simple alternative mechanism that is almost uniformly effective over a large range of frequencies, and is free of oscillating mechanical parts.

So far, many efforts have been reported on the control of flow separation over airfoils with rounded leading edges. Herein we report on the control of separated flow over sharp-edged airfoils, a topic that has not received much attention so far. There are two important differences between the actuator requirements for the two cases. First, the location of the actuators for the control of separation over rounded airfoils is not as critical, because the flow is still receptive to an external disturbance, whereas for the control of separated flow the actuation must interact with the free-shear layer to be effective. This fact dictates that the actuator of a sharp-edged wing must be as close as possible to the leading edge, which leads to the second important difference. The actuation mechanism must be adjusted to direct the disturbance as much as possible along the free-shear layer. The two parameters that characterize the effect of actuators are the momentum coefficient C_μ and the frequency of the disturbance. Different angles of attack and freestream velocities require a wide range of possible combinations of these parameters. Being able to independently control both is a great challenge. These requirements may appear too stringent for the sharp-edged airfoils but on the other hand, they may provide some opportunities for robust control with minimal energy input. The free-shear layers would be more receptive to actuation if the input is as close as possible to the location of their formation, which is the sharp leading edge. This was clearly demonstrated for the control of asymmetric wakes over pointed bodies of revolution at high incidence, which is a similar example of controlling separated flow. In this case, minute disturbances very close to the apex can feed into the global instability of the flow and lead to very large wake asymmetries as shown by Zilliac et al. [14] and Zeiger et al. [15]. In the present paper we describe an actuator that we developed, which is effective for a wide range of frequencies and allows for the independent adjustment of the momentum coefficient. We then discuss the effectiveness of this actuator in controlling the separated flow over a sharp-edged wing.

II. Experimental Setup and Equipment

Measurements were carried out in two wind tunnels, a small wind tunnel located in the Engineering Science and Mechanics (ESM) Fluids Laboratory and a large one, the VA Tech Stability Tunnel. Experiments were carried out with the same model in both tunnels. The data obtained in the ESM Wind Tunnel indicated similar trends with those presented in this paper, even though they correspond to Reynolds numbers the order of 20,000, but the blockage was non-negligible.

The Virginia Tech Stability wind tunnel is a continuous, closed-loop, subsonic wind tunnel. The maximum achievable flow speed is 84 m/s (275 ft/s) in a 1.83 m × 1.83 m × 7.62 m (6 ft by 6 ft by 25 ft) test section. This facility was constructed in 1940 at the present site of NASA Langley Research Center by NASA's forerunner, NACA, and in 1959, it was moved to Virginia Tech. Use of the tunnel at Langley to determine aerodynamic stability derivatives lead to its current name. The tunnel fan has a 14 ft (4.27 m) diameter and is driven by a 600 hp motor. The settling chamber has a contraction ratio of 9 to 1 and is equipped with antiturbulence screens. This combination provides an extremely smooth flow in the test section. The turbulence level varies from 0.018 to 0.07% and flow angularities are limited to 2 deg maximum.

The tunnel freestream velocity is obtained by a Pitot tube mounted on one of the side walls, which is connected to the data-acquisition system as well as an Edwards-Datametrics Barocel precision transducer model 590D-100T-3Q8-HSX-4D, and this in turn is connected to a 1450 Electronic Manometer that provides a readout of the dynamic pressure. The Barocel has a range of 0–100 Torr with an accuracy of 0.05% of the pressure reading and a full-scale resolution of 0.001%

A symmetric, circular-arc airfoil, $12\frac{1}{2}\%$ chord thickness was designed and constructed, with a chord length of 40.64 cm (16 in.), and a span of 53.34 cm (20 in.). It was built in two separate modules: the jet actuator/leading-edge wedge and the main body of the airfoil (Fig. 1).

The main body of the airfoil was made entirely of aluminum and consists of three holding ribs and two sheets that serve as the skin.

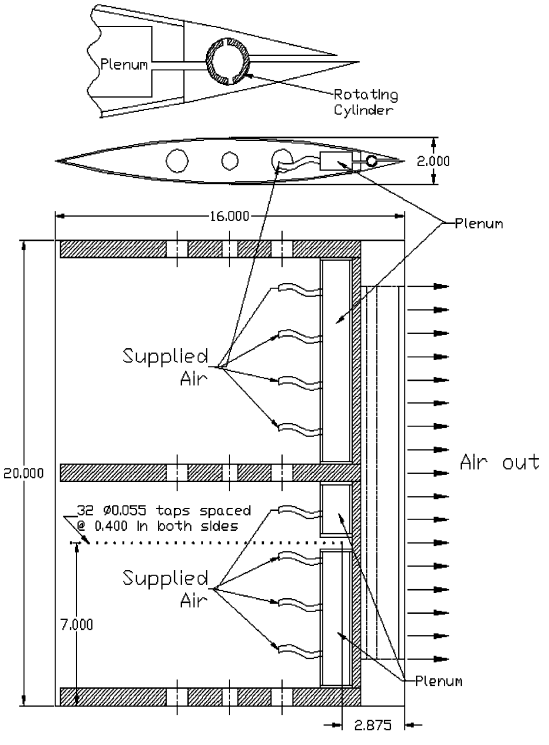

Fig. 1 Wind tunnel model schematic.

The ribs have holes that provide access to the inside. Each side has 32 pressure taps aligned in the streamwise direction, and located at 177.8 mm (7 in.) from the starboard side. The taps start at 63.5 mm ($2\frac{1}{2}$ in.) from the leading edge and are spaced at 10.16 mm (0.4 in.) intervals along the chord. Stainless steel tubing of 1.27 mm (0.05 in.) o.d., 0.8382 mm (0.033 in.) i.d., and 6.35 mm (1/4 in.) in length was inserted in each tap with Tygon tubing R-3603 of 2.38125 mm (3/32 in.) o.d. and 0.79375 mm (1/32 in.) i.d. connecting them to pressure transducers.

The design of the jet mechanism was dictated by the requirement to actuate the flow as close as possible to the leading edge of the airfoil. The leading-edge part of the wing is essentially a wedge prism as shown in the top sketch of Fig. 1. The actuator was developed and tested first by Zeiger et al. [16]. It consists of two concentric cylindrical surfaces as shown in this figure, the inner rotating inside the outer, which is fixed. The inner cylinder, shown cross hatched in Fig. 1 is an 11.11 mm (7/16 in.) brass tube with eight 0.16 mm × 3.81 mm (1/16 in. × $1\frac{1}{2}$ in.) slots, with 0.16 mm (1/16 in.) spanwise separation between them. These are aligned with the axis of the cylinder and are placed along generators 180 deg apart. This cylinder is supported on three bushings and rotates about a fixed axis inside the outer cylinder, which is the cylindrical housing created by the machined wedge. One bushing was machined to fit snugly between the brass tubing and the machined leading-edge at midspan. This was done to eliminate possible warping of the tube during rotation. The shaft of the rotating cylinder was connected to a dc motor via a coupling. This motor has an operating range between 14 and 110 V dc. Because of power supply constraints maximum operating voltage was 56 V dc. The operating speed range corresponding to this voltage range is from 720 to 3780 rpm. The power supply was calibrated and manually operated to drive the cylinder at the desired speed.

High pressure air is fed into the plenum via supply tubes, as shown in Fig. 1. It is then directed through a narrow slot along the inside of the rotating cylinder. When the cylinder slots match with the fixed slots of the housing, then air is released through the duct that leads to the leading edge of the wedge, that is, the leading edge of the wing.

To evaluate the capabilities of the actuator, a rake of high-frequency-response Pitot tubes was mounted in front of the assembled leading-edge device. Endevco model 85102 pressure transducers were used as sensing elements inside the rake. These have a range of 0–2 psi, sensitivity of 106 mV/ps and resonance frequency of 70 kHz. The output of the pressure transducers was connected to a HP digital signal analyzer, which was used to measure jet frequencies. In addition, these were also connected to a simple PC-driven 12-bit data acquisition system. The rake was mounted on traversing scales, so that it could easily be displaced to obtain data at different locations relative to the slotted nozzle.

The pressure transducers used to record the surface pressure over the model were Pressure Systems, Inc. ESP pressure scanners. These scanners are small, high-density packages, containing multiple differential sensors. Each channel is a minipiezoresistive pressure transducer with output internally amplified to ±5 V full scale. These transducers have an accuracy of 0.10% of full scale after full calibration and a frequency response of 50 Hz. The transducers reference pressure was the freestream static pressure. Two 32-channel scanners were employed. The last port in the second ESP was set aside for the tunnel total pressure.

The ESP scanners were mounted inside the model in order to reduce the pressure attenuation effects induced by the tubing. The scanners were connected to dedicated boards for digital addressing as well as voltage regulation and were sampled at 250 Hz. Sampling was carried out with a data acquisition board from Computer Boards model CIO-DAS08 12-bit A-D converter installed on an 800 MHz Pentium III processor. The Endevco pressure transducers were connected to the same setup system, although their inputs were acquired as external sources, and they were calibrated every 30 min of operation.

The uncertainty for each pressure measurement is ±4.981 Pa, which is equivalent to a c.p. uncertainty of ±0.08669. In all cases, the length of the tubing connections never exceeded 38 cm (15″). It has been shown that for this type and length of tubing, the pressure attenuation and phase difference at the transducers are very small for input frequencies up to 25 Hz. Even for a frequency of 50 Hz the response of the ESP units can be realized with an amplitude response of 1.018, whereas the phase lag could be as high as 10 deg. But in our case phase lag does not affect the conclusions we draw from our investigation. The propagation of error from measured to calculated quantities indicates that integrating over a discrete number of points, N, in this case the points of pressure taps over the airfoil, introduces a factor of $N^{-1/2}$. The error in determining the lift coefficient was thus estimated to be $\delta C_L = 0.0453$.

III. Jet Characterization

Actuation calibration was carried out to document actuator response under different conditions, and in particular, to explore possible coupling between the actuating frequency and the jet velocity amplitude, which is the case with piezoelectric actuators. Moreover, we needed to document how the asymmetry of the nozzle geometry affects the jet velocity profile.

Traversing scales driven by stepper motors and controlled by the data-acquisition system were used to place the rake at different positions along the leading-edge slot, and perpendicular to the slot. Velocity profiles were thus generated. We tested the actuator at supply pressures ranging from 40 psi to 100 psi and frequencies between 15 and 63 Hertz.

Power spectra of the recorded signals (Fig. 2) obtained with the cylinder driven at 31.5 Hz, revealed that the dominant frequency of the jet was twice the driving frequency of the motor. This was expected, because the rotating cylinder has two slots and therefore generates two jets with one revolution. The spectrum confirmed that no secondary motions were generated by nonlinear interactions, because the only other visible frequency was the first harmonic of the actuation frequency, and therefore this device could generate pulsed jets with any desired frequency, without introducing unwanted frequencies.

The basic hypothesis here is that this actuator can produce pulsing jets with amplitudes independent of the driving frequency. To test this hypothesis, we measured the Pitot amplitudes at five locations along the span of the slot nozzle for a range of driving frequencies and for a fixed plenum pressure of 100 psi. At each spanwise position, the instrument was placed at the point of maximum reading. These data were obtained by Zeiger et al. [16] and were reported only in terms of the pressure transducer voltage. The results were not reduced to velocity at that time and for this reason they are not included in this paper. The amplitudes presented in Zeiger et al. [16] indicate a mild dependence on the driving frequency. Such measurements were repeated a year later [17] and the results reduced to velocities are shown in Fig. 3, indicating that the amplitude is indeed independent of the driving frequency. Other data reported in Rullan et al. [17] indicate that the amplitudes of the pulsing jets are increasing with the plenum pressure.

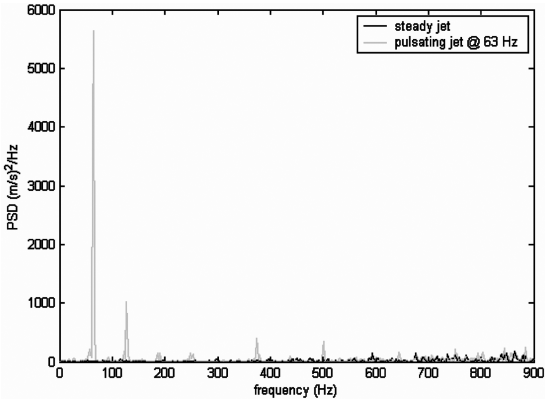

Fig. 2 Power spectrum for steady jet and for 63 Hz pulsating jet with the same pressure.

Velocity profiles at different downstream distances across the steady jet were plotted in terms of coordinates shown in Fig. 4. The results presented in Fig. 5 for steady flow indicate that the location of the maximum velocity is mildly displaced upward, that is, in the direction of the short side of the nozzle. This implies that the jet deviates from the direction of the z axis. The upward displacement is not as pronounced if the data are plotted versus the similarity independent variable of $y/z^{2/3}$. The maximum velocity of the first profile is used to nondimensionalize all velocity profiles presented here. This is the profile measured at the lower edge of the slot for the steady jet.

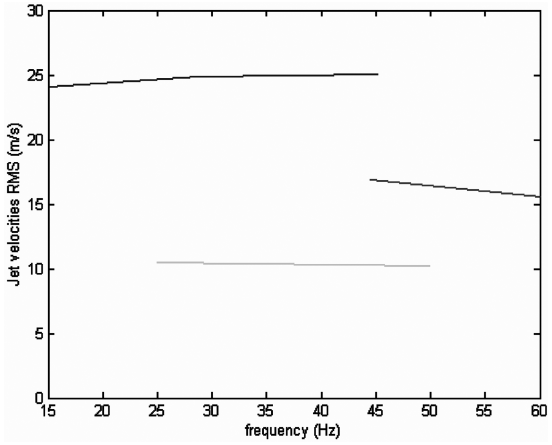

Fig. 3 Amplitude as a function of applied pressure and frequency. Top curve: 100 psig; middle: 80 psig; bottom curve: 25 psig.

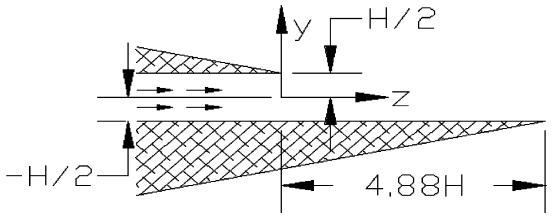

Fig. 4 Sketch of coordinate system for velocity profiles.

Averaged profiles for the pulsed jet are presented in Figs. 6 and 7 for driving frequencies of 15 and 45 Hz, respectively. The maximum velocity is considerably higher that the corresponding value of the steady jet. This may be attributed to steady streaming, a nonlinear mechanism that enhances the average of a pulsing stream if a pressure gradient is present. In these profiles, the upward vectoring of the jet is more pronounced. This tendency of deviation from the axial direction of the duct can be attributed to the asymmetry of the nozzle. As shown in Fig. 4, one side of the jet duct is shorter than the other. As a result, the boundary layer on one side becomes a free-shear layer before the layer on the other side. Thus on one side, the free vorticity may start rolling, whereas the shear layer on the other side is constrained by the flat solid wall, and vorticity retains its organization in the form of a flat wall boundary layer. Rolled vortices generate regions of low pressure and thus induce changes in the direction of the jet. To confirm these phenomena, we obtained detailed PIV measurements in the immediate neighborhood of the actuator slot. A representative instantaneous frame is presented in Fig. 8. In this Figure it is clear that a disturbance is turning up and away from the wall jet in a manner more pronounced than by the velocity profiles measured and presented. It is perhaps this vortex that induces the upward bending of the jet.

Apparently, this effect is not as pronounced for steady flow. This is expected, because the distance the free-shear layer travels before the other side becomes free is short. For such a distance, no large vortical structures can grow. The situation is different with pulsing jets. An unsteady jet starting from rest quickly rolls into two large vortices in two dimensions, or a vortex ring in axisymmetric flow as suggested by Didden [18] and Glezer [19]. In our case, the asymmetry of the two flat sidewalls allows the formation of a vortex on one side but forces vorticity to be confined in an attached boundary layer on the other side. The vortex being formed only on one side induces a low pressure, and deflects the flow away from the long wall as indicated in Fig. 8. In addition, the increase in frequency does not change further the velocity profiles with respect to the steady blowing case, indicating that this further vectoring is a result of the pulsation

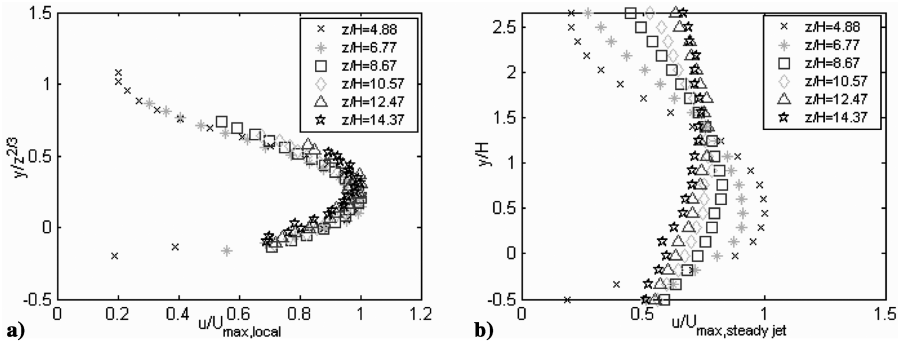

Fig. 5 Steady Jet velocity profile a) self-similar, b) standard coordinates.

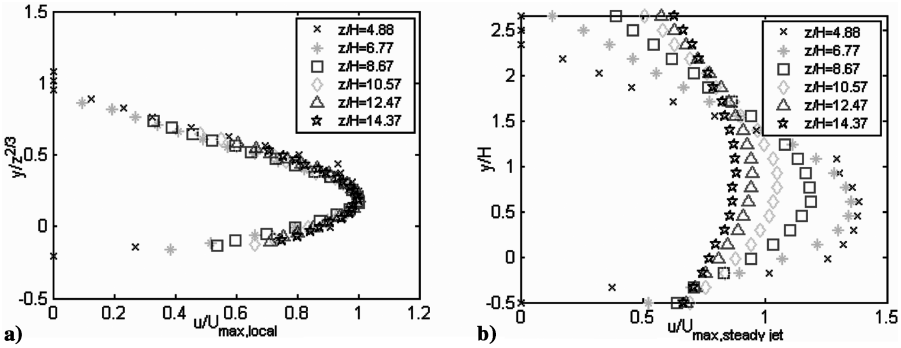

Fig. 6 Mean velocity profile. Jet Pulsating at 15 Hz, a) self-similar, b) standard coordinates.

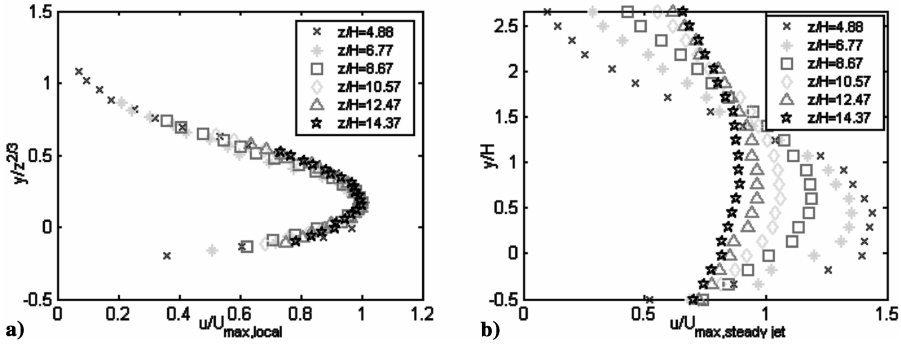

Fig. 7 Mean velocity profile. Jet Pulsating at 45 Hz, a) self-similar, b) standard coordinates.

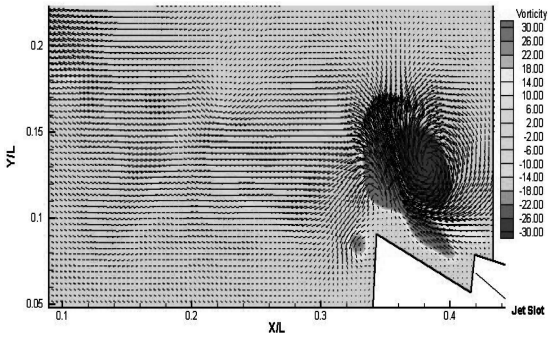

Fig. 8 Instantaneous PIV data (velocity vectors and vorticity contours) for the jet issuing from the leading edge slot. Negative vorticity (clockwise) is released sooner and thus rolls before negative vorticity.

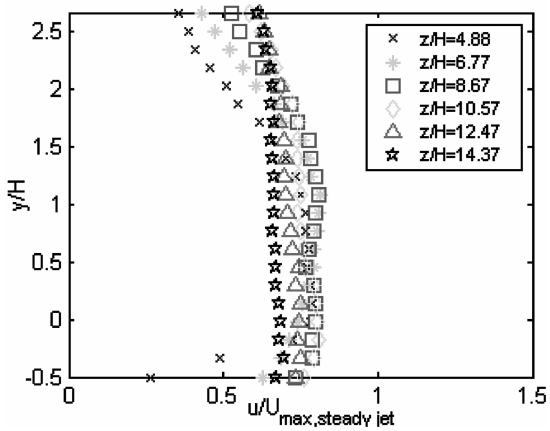

Fig. 9 Rms velocity profile. Jet Pulsating at 15 Hz.

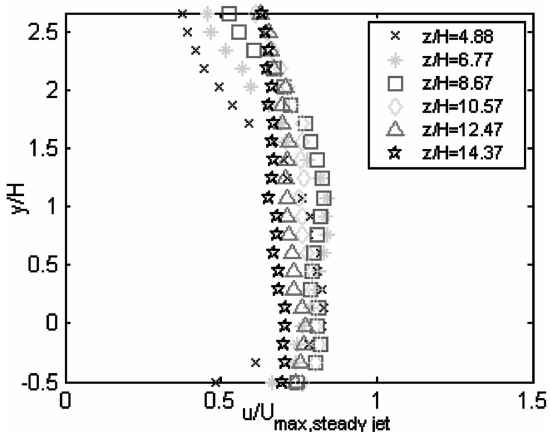

Fig. 10 Rms velocity profile. Jet Pulsating at 45 Hz.

without regard to magnitude or frequency. More PIV data on the vectoring effects obtained with PIV were presented in Rullan et al. [17], and will be included in a subsequent publication.

In Figs. 9 and 10 we present the rms of the jet velocities along the same downstream stations. We observe in these figures that the amplitude of the unsteady part of the profiles is almost independent of the spanwise distance. Moreover we calculated that the magnitude of the rms velocity is larger than the mean of the steady part.

IV. Pressure Distributions

The model was tested in the two tunnels described above at low and moderate Reynolds numbers, with and without actuation. Data obtained in the ESM tunnel at Reynolds numbers the order of 20,000 were reported in [17]. Here we present data obtained at a Reynolds number the order of 300,000 in the VA Tech Stability Tunnel and originally reported in [20]. Actuation was characterized by the momentum coefficient and the pulsation frequency. The momentum coefficient here is defined as

$$C_\mu = \frac{\rho_{\text{jet}} u_{\text{jet}} H}{\rho_\infty U_\infty c \sin\alpha}$$

This is the ratio of the input momentum to a nominal momentum of the freestream and is suggested in Wu et al. [21] that it should to be at least 1%. In the present case both the jet and the freestream have Mach numbers much lower than 0.3 and thus their respective densities cancel out. The momentum coefficients reported here are based on the rms of the maximum jet velocity, which is the quantity mostly affecting the flow, and usually reported in literature. It should be noted here that the jet delivered by this actuator is not a zero-mass jet. Synthetic jets are zero-mass devices right at their orifice. But a few orifice diameters downstream, they too are characterized by a jet with a significant mean component. So our jet is not much different from a jet delivered by a synthetic jet actuator. We estimated that the momentum coefficient based on the velocity averaged over the slot and over time is about 70% of the momentum coefficient based on the rms velocity.

The disturbance frequency likely to be amplified the most is the Strouhal frequency, which in dimensionless form is given by the Strouhal number $St = f_{\text{shedding}} c \sin\alpha / U_\infty$. Note that we are introducing sine(α) into the Strouhal number, because shedding is affected by the vertical projection of the airfoil as seen in Miranda et al. [1,2]. We are going to assume a value of $St = 0.2$ for this research as is widely accepted in literature. Our tests in a water tunnel and two wind tunnels with sharp-edged wings at incidence confirmed that this value is within 0.015, for a range of Reynolds numbers form 10,000 to a million. We report our results in terms of the normalized ratio $F = f_{\text{actuation}} / f_{\text{shedding}}$. Seifert et al. [6] define a dimensionless frequency, F^+, using the freestream velocity and the chord length. They suggest that this reduced frequency should be in the range of $0.4 < F^+ < 2$ because it seems that harmonics play a role in the dynamic process. It is unfortunate that researchers of flow-induced vibrations use the symbol F^+ to denote the ratio we call F.

Experiments were carried out in the VA Tech Stability Wind Tunnel. In this tunnel, our model arrangement corresponds to a

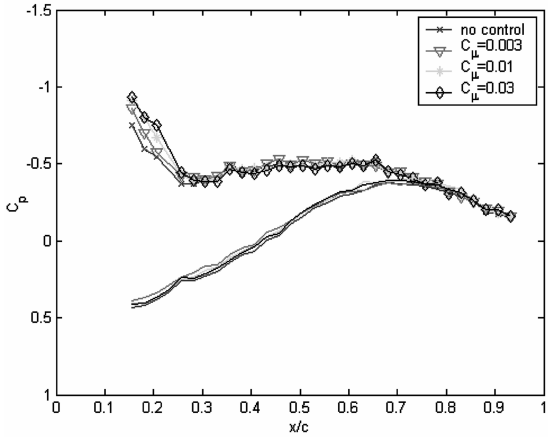

Fig. 11 Averaged pressure distributions at $\alpha = 3$ deg.

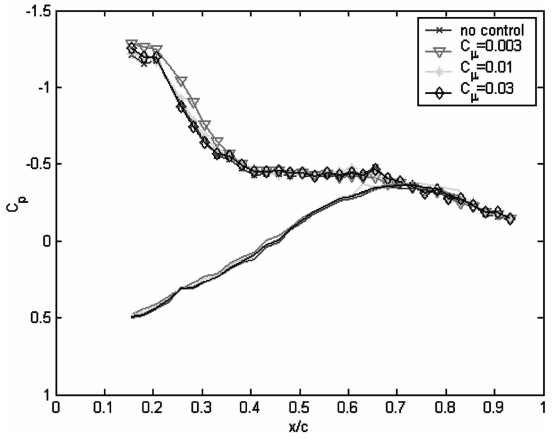

Fig. 12 Averaged pressure distributions at $\alpha = 6$ deg.

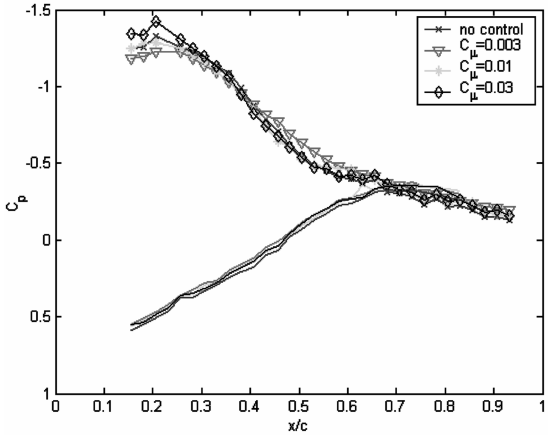

Fig. 13 Averaged pressure distributions at $\alpha = 9$ deg.

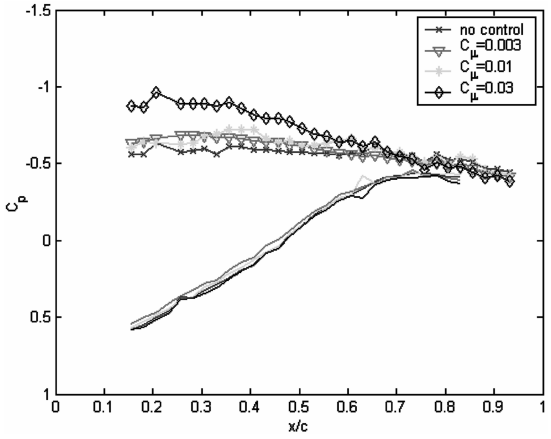

Fig. 14 Averaged pressure distributions at $\alpha = 12$ deg.

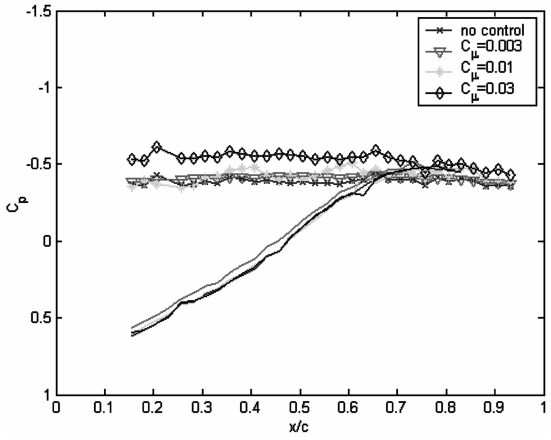

Fig. 15 Averaged pressure distributions at $\alpha = 15$ deg.

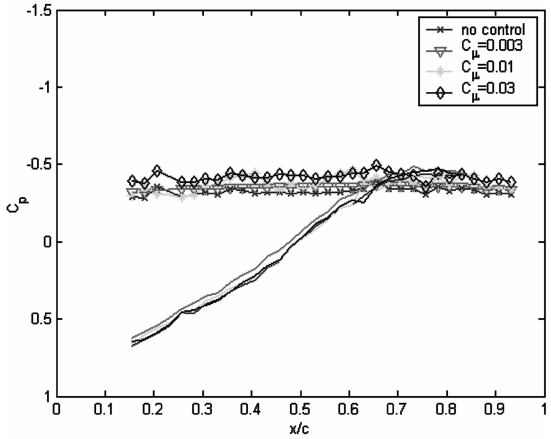

Fig. 16 Averaged pressure distributions at $\alpha = 18$ deg.

blockage coefficient of 2.2% for an angle of attack of 21 deg, which was the largest one tested. These tests can therefore simulate well the case of a wing in an infinite domain. The model was equipped with flat end plates to reduce as much as possible the end effects. This technique generates fields that are closer to two-dimensional flow, than if the model were to be attached to the tunnel walls. This is because boundary layers growing on long walls are thick and interact with the flow near the roots of the airfoil, giving rise to thick horseshoe vortices. Tests were carried out at angles of attack of 3 deg up to 21 deg, in increments of 3 deg. Also three different C_μ's were tested, namely 0.003, 0.01 and 0.03. Because of motor as well as air pressure supply limitations, the runs for different C_μ's were done at different tunnel speeds and thus slightly different Reynolds numbers. Our results suggest that in this range of Reynolds numbers the pressure coefficients measured at different Reynolds numbers differ by less than 1.5%.

Average pressure measurements over the chord of the airfoil for these angles of attack are shown in Figs. 11–17. The actuation device was pulsated at the shedding frequency of the airfoil for each angle of attack. These correspond to 98.15 Hz for $\alpha = 3$ deg, 49.14 Hz for $\alpha = 6$ deg, 32.84 Hz for $\alpha = 9$ deg, 24.7 Hz for $\alpha = 12$ deg, 19.84 Hz for $\alpha = 15$ deg, 16.62 Hz for $\alpha = 18$ deg, and 14.33 Hz for $\alpha = 21$ deg. Because it was very difficult to place pressure taps on the leading wedge, we were not able to obtain pressure data very near the leading edge of the wing. In all these figures, special symbols characterize the suction side values for

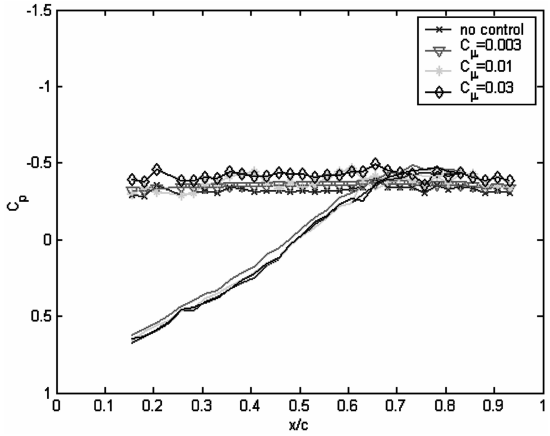

Fig. 17 Averaged pressure distributions at $\alpha = 21$ deg.

different C_μ values. But the curves on the pressure side are so close to each other that similar parameter designation would be impossible to read.

For $\alpha = 3$ deg (Fig. 11), there is a peculiar sharp pressure drop near the leading edge on the suction side. This Cp curve appears rising, because we are plotting negative values. We believe that this is due to a separated bubble near the leading edge. But this bubble is not the type of bubble observed at moderate Reynolds numbers over airfoils with rounded leading edges. The latter are very short and shallow, because with an inflectional velocity profile, the flow transitions to turbulence, and reattaches almost immediately. The separated bubble in the present case covers about 30% of the airfoil. Similar pressure distributions were obtained by Cahil et al. [22] over a sharp-edged wing but with a lower thickness ratio.

Our control mechanism is not effective at $\alpha = 3$ deg and 6 deg (Figs. 11 and 12), a behavior we expected, because the flow is attached over most of our relatively thick wing. However, the control actuation again lowers the pressure levels in the very front of the airfoil, where the separation bubble resides. The actuation is not very effective even at $\alpha = 9$ deg, as shown in Fig. 13; although there is now clear indication of the effect near the leading edge. But at $\alpha = 12$ deg (Fig. 14), we observe some significant departures from the no-control case. The comparison of the data of the latter two figures indicates that the flow at $\alpha = 9$ deg displays a distribution similar to those over airfoils with rounded leading edges. The suction side pressure has its extreme values very near the leading edge. Suction is reduced as we move towards the trailing edge. But for $\alpha = 12$ deg, the no-control case indicates a flat pressure distribution on the suction side. This is clear indication that the flow is massively separated. And yet, much like the case of control with oscillating miniflaps (Miranda et al. [1]), actuation at the leading edge brings the pressure distributions closer to those of attached flow, namely, the pressure is lowered near the leading edge and rises near the trailing edge. This is deceiving, because the flow is still separated. It is only in the average that the pressure distribution is similar to the distribution of attached flow. The effect is more pronounced with higher levels of C_μ.

In Figs. 15–17 for $\alpha = 15$, 18, and 21 deg, respectively, the effect of flow control is not as large, and in fact, it is progressively reduced as the angle of attack is increasing. It may be possible to achieve greater reductions on the suction side with larger values of C_μ, but due to limitations expressed before, such tests could not be performed.

Lift and drag coefficients were calculated by integrating the pressures over the suction and pressure sides of the wing. Local pressure values are multiplied with the corresponding length increment and the cosine or sine of the angle of inclination of the airfoil surface to return lift and drag. The effects of skin friction are not included in these estimates. Calculations required extrapolation of the data near the leading edge. This extrapolation results in underestimating the suction near the leading edge. The results are presented in Table 1, for the three values of C_μ as well as for no control. The benefit on the lift coefficient is large in the post-stall area, but it is reduced as the angle of attack is increased. This is seen in the last column, which is a comparison between the no-control case and the control case with the highest C_μ.

Table 1 Lift coefficient C_L for $Re = 270,000$

AOA	No control	$C_\mu = 0.003$	$C_\mu = 0.01$	$C_\mu = 0.03$	Increase in C_L
3	1.0662	1.0612	1.1057	1.1570	5%
6	1.6481	1.7007	1.5986	1.6514	−0.23%
9	2.1067	1.9899	2.0038	2.1308	1.91%
12	1.3847	1.4135	1.4376	1.8110	28.41%
15	0.9370	0.8984	0.9708	1.2760	31.85%
18	0.8720	0.8328	0.9282	1.0575	24.22%
21	0.8952	0.8772	0.9343	0.9931	13.76%

Table 2 Lift-to-drag ratio, C_L/C_D for $Re = 270,000$

α	No control	$C_\mu = 0.003$	$C_\mu = 0.01$	$C_\mu = 0.03$	Increase in C_L/C_D
3	7.2248	7.9616	8.0992	8.1356	12.6%
6	9.3634	10.65213	9.2264	9.3714	2.8%
9	7.5310	6.9529	7.1952	7.5868	0.74%
12	3.0834	3.3201	3.1875	3.8473	24.77%
15	2.1611	2.1575	2.1483	2.4982	15.60%
18	1.8374	1.8156	1.8567	1.9781	7.65%
21	1.6635	1.6381	1.6524	1.7168	3.20%

The pattern previously discussed is also evident in Table 2, in which we display the lift-to-drag ratio for the same conditions. Here the increase is not as pronounced as it is for the lift coefficient. This indicates that drag is increasing as well. The vortex lowers the pressure over the surface but the force obtained is normal to the surface. When the angle of attack is further increased, the component of the normal force in the direction of the drag is increased as well and the lift component is reduced. This situation could be addressed by keeping the vortex closer to the front of the airfoil and detaching it farther from the trailing edge as the angle of attack is increased. In this way we could take advantage of the airfoil curvature.

A control jet issuing against the freestream actually contributes to drag. We estimated that this contribution varies between 1 and 2% in the range of angles of attack tested. The larger values actually correspond to the low angles of attack. But in practice, the control mechanism suggested here would not be employed in cruising. It would be useful in takeoff and landing or in the execution of sharp maneuvers. And in these cases, 2% of more drag may not be a serious detriment, and on occasion it may prove beneficial.

It is emphasized that the data presented so far are averaged pressure distributions. We average over both the periodic and the random fluctuations of the signals. Instantaneous pressure distributions over the wing at four specific consecutive instances are presented in Fig. 18. These data provide evidence that large vortices are convected over the airfoil. It appears that a dominant vortex forms and convects, inducing in the process an imprint of a traveling wave of very low pressure. This is evident in the instantaneous curves presented in Fig. 18. For $t = 0$, we observe a dominant negative trough at about $x/c = 0.4$. It appears that this trough, which we interpret to be the imprint of a traveling vortex, is displaced downstream as time progresses, and at $t = 0.024$ sec, it is located at $x/c = 0.75$, close to the trailing edge as a new trough emerges near the leading edge. This gives an approximate speed of propagation for the wave of 5.6 m/s, whereas the freestream velocity is $U_\infty = 10$ m/s, which corresponds to a vortex-shedding frequency of 24.85 Hz. The power spectrum of the signals from ports located between $x/c = 0.15$ and $x/c = 0.7$ indicate a dominant frequency at 25.4 Hz as shown in Fig. 19 which shows the power spectrum for port 4 located at $x/c = 0.23$. This corroborates the earlier estimate of the shedding frequency. Power spectra of signals from other ports located at $x/c > 0.75$ showed no dominant frequency, implying that

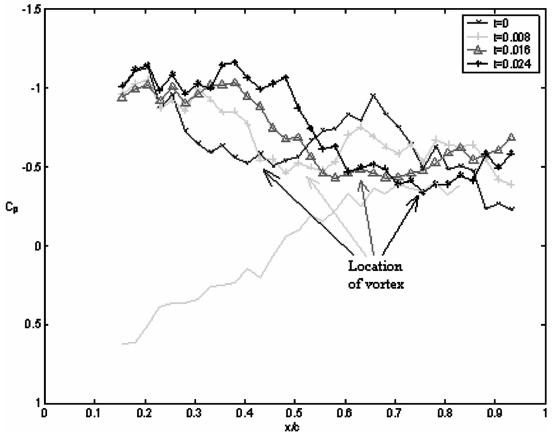

Fig. 18 Instantaneous pressure distributions over the airfoil for $\alpha = 12$ deg and $C\mu = 0.03$: time values in seconds.

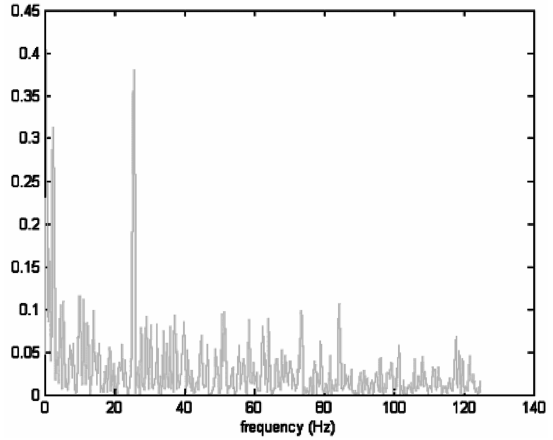

Fig. 19 PSD for port 4 signal at $\alpha = 12$ deg with no control.

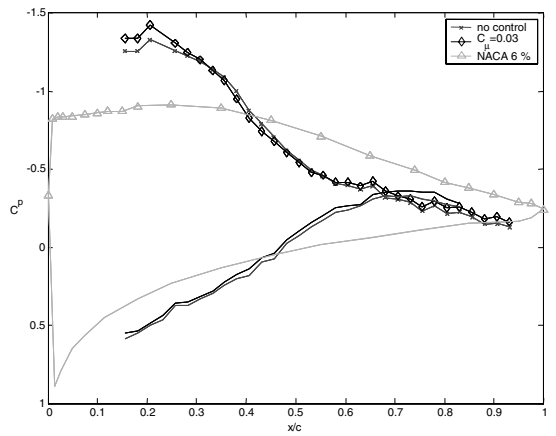

Fig. 20 Comparison between NACA airfoil and stability results at $\alpha = 9$ deg.

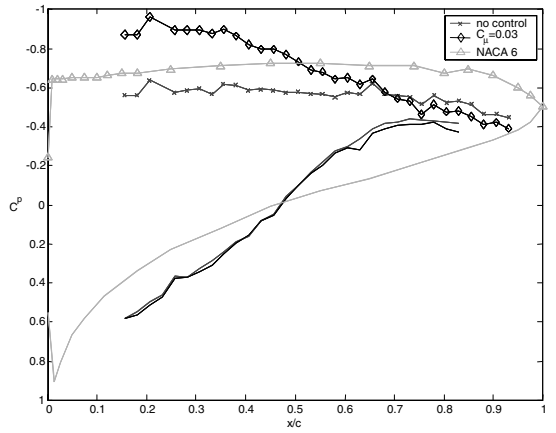

Fig. 21 Comparison between NACA airfoil and stability results at $\alpha = 12$ deg.

the vortex probably detached from the surface at approximately $x/c = 0.75$. This suggests that the vortex convects over 75% of the suction side and then lifts off.

It is useful to compare the data of Cahil et al. [22] with the present results, although just for reference, because their thickness ratio was 0.06 as compared with 0.125 for the present study. Cahil et al. experimented with a circular-arc airfoil equipped with large, hinged leading and trailing-edge flaps. Similar flaps are employed by fighter aircraft, in order to increase lift during takeoff and landing. It is therefore appropriate to compare the effect of a large leading-edge flap, to the effects of flow control. For $\alpha = 9$ deg (Fig. 20), the Cahil et al. data for no control indicate that the flow is fully separated, whereas the flow over our airfoil with no control appears to be still attached. This can be attributed to the wings' different thickness ratios. With only 6% thickness ratio, the Cahil et al. airfoil behaves aerodynamically like a flat plate, and thus at $\alpha = 9$ deg, the flow over such an airfoil is separated, displaying a nearly flat pressure distribution on the suction side. But with a thickness ratio of 12.5%, the flow over our airfoil at this incidence stays attached, and for this reason, flow control does not provide any significant improvement. The mild improvement near the leading edge could be attributed to virtual reshaping that our pulsed jet may be inducing. This could be equivalent to "blunting" of the leading edge, as indicated in [23,24]. At $\alpha = 12$ deg on the other hand, the flow over the 12.5% airfoil is also separated, and as shown in Fig. 21, our data display pressure distributions very similar to those presented in [22]. Now, flow control influences the flow field and thus the pressure distribution. But the flow is fully separated, as detected by instantaneous pressure distributions shown in Fig. 18. Unfortunately, Cahil et al. [22] do not present pressure distributions for wings with deployed flaps. It is therefore not possible to compare the effect of flow control with that of deploying a large flap. We have made such comparisons earlier [2] that proved that the effect of flow control is almost identical to the effect of drooping large flaps. But flow control by Miranda et al. [2] was achieved by oscillating miniflaps.

V. Conclusions

One of the purposes of this research was to develop a flow control mechanism that could generate a pulsing jet along a slotted nozzle to increase the lift of circular-arc airfoils. A novel pulsing jet actuator was designed and constructed. A feature of this device is that it can generate oscillating disturbances without any linearly or radially oscillating mechanical parts like a piston or an oscillating flap. Another feature is that the effectiveness of this actuator is nearly independent of the frequency. Finally, this actuator does not generate nonlinear interactions and therefore any secondary frequencies as synthetic jets tend to do. This means that the device is a good candidate for a robust flight actuator, where the required actuation frequency and mass flow are changing with aircraft speed and angle of attack. The location and geometry of the jet exit revealed that the asymmetry of the nozzle shape induces the formation of a small starting vortex. This vortex provides a vectoring effect that guides the disturbance in the direction of the leading-edge free-shear layer.

We demonstrated for the first time, that unsteady blowing right at the leading-edge of a sharp-edged, circular-arc airfoil allows the management of the separated flow, leading to averaged pressure distributions that result in higher lift. This was shown to be due to convecting vortices, as detected in the form of a low-pressure traveling wave. Increases as high as 30% were obtained in the lift coefficient, for moderate angles of attack. Corresponding increases of the lift-to-drag ratio were lower, the order of at most 25%, because drag also increases with leading-edge control. But the effect

decreased as the angle of attack was increased beyond 15 deg, possibly due to less effective interaction between the disturbance and the shear layer. The data obtained with unsteady blowing indicate that there is a minimum of energy needed in order to exert a proper disturbance on the shear layer. In addition, the results suggest that the harmonics of the natural shedding frequency can have even greater impact than the natural frequency. Finally, the actuating frequency did not have to match the natural frequency. Apparently, the hydrodynamics lock on to the driving frequency, as demonstrated previously by the authors [1,2].

Acknowledgments

This work was supported by the Air Force Office of Scientific Research, under Grant No. FA9550-04-1-0144, Rhett W. Jefferies, monitor. Carl Tillman is our point of contact at Air Force Research Labs. We appreciate their interest in our work and their support.

References

[1] Miranda, S., Telionis, D., and Zeiger, M., "Flow Control of a Sharp-Edged Airfoil," AIAA Paper No. 2001-0119, Jan. 2001.

[2] Miranda, S., Vlachos, P., Telionis, D., and Zeiger, M., "Flow Control of a Sharp-Edged Airfoil," *AIAA Journal*, Vol. 43, No. 4, 2005, pp. 716–726.

[3] Zhou, M. D., Fernholz, H. H., Ma, H. Y., Wu, J. Z., and Wu, J. M., "Vortex Capture by a Two-Dimensional Airfoil with a Small Oscillating Leading-Edge Flap," AIAA Paper 93-3266, 1993.

[4] Hsiao, F.-B., Wang, T.-Z., and Zohar, Y., "Flow Separation Control of a 2-D Airfoil by a Leading-Edge Oscillating Flap," *Pacific International Conference on Aerospace Science Technology*, Vol. 1, National Chong Kung University, Taiwan, ROC, 1993, pp. 250–256.

[5] Hsiao, F. B., Liang, P. F., and Huang, C. Y., "High-Incidence Airfoil Aerodynamics Improvement by Leading-Edge Oscillating Flap," *Journal of Aircraft*, Vol. 35, No. 3, 1998, pp. 508–510.

[6] Seifert, A., Bachar, T., Koss, D., Shepshelovich, M., and Wygnanski, I., "Oscillatory Blowing: A Tool to Delay Boundary-Layer Separation," *AIAA Journal*, Vol. 31, No. 11, 1993, pp. 2052–2060.

[7] McManus, K., and Magill, J., "Separation Control in Incompressible and Compressible Flows Using Pulsed Jets," AIAA Paper 96-1948, 1996.

[8] Seifert, A., and Pack, L. G., "Active Control of Separated Flows on Generic Configurations at High Reynolds Numbers," AIAA Paper 1999-3403, 1999.

[9] Glezer, A., and Amitay, M., "Synthetic Jets," *Annual Review of Fluid Mechanics*, Vol. 34, Palo Alto, California, Jan. 2002, pp. 503–529.

[10] Cattafesta, L. N., Garg, S., and Shukla, D., "Development of Piezoelectric Actuators for Active Flow Control," *AIAA Journal*, Vol. 39, No. 8, 2001, pp. 1562–1568.

[11] Chen, F.-J., Yao, G. B., Beeler, G. B., Bryant, R. G., and Fox, R. L., "Development of Synthetic Jet Actuators for Active Flow Control at NASA Langley," AIAA Paper No. 2000-2405, June 2000.

[12] Schaeffler, N. W., "The Interaction of a Synthetic Jet and a Turbulent Boundary Layer," AIAA Paper No. 2003-0643, 2003.

[13] Gilarranz, J. L., and Rediniotis, O. K., "Compact, High-Power Synthetic Jet Actuators for Flow Separation Control," AIAA Paper 2001-0737, 2001.

[14] Zilliac, G. G., Degani, D., and Tobak, M., "Asymmetric Vortices on a Slender Body of Revolution," AIAA Paper No. 1990-0388, Jan. 1990.

[15] Zeiger, M. D., and Telionis, D. P., "Effect of Coning Motion and Blowing on the Asymmetric Side Forces on a Slender Forbody," AIAA Paper No. 97-0549, 1997.

[16] Zeiger, M. D., Gerlach, J. M., Vlachos, P. P., and Telionis, D. P., "Frequency-and-Amplitude-Independent Flow Controller for Sharp-Edged Wings" AIAA Paper No. 2002-0969, Jan. 2002.

[17] Rullan, J., Vlachos, V., Telionis, D., and Zeiger, M., "Post-Stall Flow Control of Sharp-Edged Wings via Unsteady Blowing," AIAA Paper No. 2003-0062, 2003.

[18] Didden, N., "On the Formation of Vortex Rings: Rolling Up and Productions of Circulation," *Zeitschrift fur Angewandte Mathematik und Physik* Vol. 30, No. 1, 1979, pp. 101–106.

[19] Glezer, A., "The Formation of Vortex Rings," *Physics of Fluids*, Vol. 31, No. 12, 1998, pp. 3532–3542.

[20] Rullan, J. M., Vlachos, P. P., Telionis, D. P., and Zeiger, M. D., "Flow Control of Sharp-Edged Wings via Unsteady Blowing," AIAA Paper No. 2004-0226, 2004.

[21] Wu, J. Z., Lu, X.-Y., Denny, a. G., Fan, M., and Wu, J.-M., "Post Stall Flow Control on an Airfoil by Local Unsteady Forcing," *Journal of Fluid Mechanics*, Vol. 371, Sept. 1998, pp. 21–58.

[22] Cahill, J. F., Underwood, W. J., Nuber, R. J., and Cheesman, G. A., "Aerodynamics Forces on Symmetrical Circular-Arc Airfoils with Plain Leading-Edge and Plain Trailing-Edge Flaps," NACA, Rept. 1146, 1953.

[23] Amitay, M., Horvath, M., Michaux, M., and Glezer, A., "Virtual Aerodynamic Shape Modification at Low Angles of Attack using Synthetic Jet Actuators," AIAA Paper 2001-2975, 2001.

[24] Chatlynne, E., Rumigny, N., Amitay, M., and Glezer, A., "Virtual Aero-Shaping of a Clark-Y Airfoil using Synthetic Jet Actuators," AIAA Paper 2001-0732, 2001.